Available online at www.sciencedirect.com
ScienceDirect
Journal of Colloid and Interface Science 316 (2007) 762–770
JOURNAL OF Colloid and Interface Science
www.elsevier.com/locate/jcis

Structure and size of spontaneously formed aggregates in Aerosol OT/PEG mixtures: Effects of polymer size and composition

M. Mercedes Velázquez [a,*], Margarita Valero [a], Francisco Ortega [b], J. Benito Rodríguez González [c]

[a] *Departamento de Química Física, Universidad de Salamanca, E-37008 Salamanca, Spain*
[b] *Departamento de Química Física I., Facultad de Ciencias Químicas, Universidad Complutense de Madrid, E-28040 Madrid, Spain*
[c] *Microscopía Electrónica de Alta Resolución y Caracterización de Materiales, C.A.C.T.I., Universidade de Vigo, E-36310 Vigo, Spain*

Received 3 May 2007; accepted 3 September 2007

Available online 7 September 2007

Abstract

Dynamic light scattering and Cryo-TEM measurements have allowed us to obtain the size and structure of spontaneous aggregates formed by mixtures of Aerosol OT, AOT, and ethylene glycol polymers of different molecular mass. The results presented in this work show that small unilamellar vesicles predominate in pure Aerosol OT solutions and in dilute polymer solutions mixed with AOT. In the latter case, elongated micelles coexist with unilamellar vesicles. When polymer concentration increases above a certain concentration, the small vesicles disappear and the size of the elongated micelles decreases to a radius compatible with spherical micelles. For PEG concentrations above the overlapping ones, spherical micelles coexist with very large aggregates probably formed by large rod like micelles or by superstructures of elongated micelles embedded in a polymer network. This behavior is consistent with theoretical models based in molecular mean-field theory [M. Rovira-Bru, D.H. Thompson, I. Szleifer, Biophys. J. 83 (2002) 2419]. The properties of the different types of aggregates are obtained by fluorescence spectroscopy and electrophoretic mobility measurements.

Keywords: Aerosol OT; Spontaneous vesicles; Poly(ethylene glycol); Nabumetone; Fluorescence probing; Electrophoretic mobility; Light scattering measurements; Cryo-TEM

1. Introduction

Vesicles and biomembranes consist of a surfactant bilayer that separates an inner region of water from a continuous phase of the same fluid. They play critical roles in compartmentalization functions as varied as nutrient transport and DNA protection [1]. Phospholipids are the natural components of cell membranes whereas synthetic surfactants form vesicles widely used in cosmetic products, in microencapsulation for drug delivery, or as anticancer agents [2]. The majority of processing methods for vesicles or liposome production use an input of energy, ultrasonic treatment, elevated temperature or pressures [3] to disperse surfactants as a vesicle phase that in most cases is unstable and highly polydisperse. However, a limited number of alternative procedures that do not use external energy sources have been described. These procedures involve surfactant mixtures, catanionic [4–6], cationic/cationic [7], nonionic/ionic [8]. These spontaneous vesicles are thermodynamically stable in contrast to the ones formed by nonequilibrium methods. The challenge in formulation is to find inexpensive stable vesicles with well-defined sizes. Spontaneous vesicle formation in mixed aggregates seems to be caused by curvature-induced asymmetry in the composition of monolayers [9]. To determine the optimal characteristics of a vesicle, complex theoretical approaches have been developed [9–12]. These models showed that a small variation in composition is enough to result in large change in the optimal size and in the existence of spontaneous vesicles.

On the other hand, it was demonstrated that the inclusion of small percentage of polymers in liposome formulations used as drug carriers increased their circulation time in vivo, favoring the uptake in the target site [13]. Their resistance to blood stream is due to steric stabilization by the polymer layer

* Corresponding author. Fax: +34 923 294574.
E-mail address: mvsal@usal.es (M.M. Velázquez).

0021-9797/$ – see front matter
doi:10.1016/j.jcis.2007.09.008

anchored on the surfactant layer [14]. One of the most common polymers used for this purpose is poly(ethylene glycol) because it is not toxic. However, PEG-lipid liposomes tend to form micelles when polymer concentration exceeds a certain concentration. This concentration decreases as the polymer molecular weight increases [15]. However, while there is a substantial body of information about the effect of polymers on the properties and stability of liposomes obtained by an input of energy less attention is directed toward the effect of polymers in spontaneously formed vesicles. Therefore, our present goal is to investigate the effect of adsorbed PEG polymers on Aerosol OT vesicles. We choose Aerosol OT because it forms spontaneous vesicles in water [16] in some surfactant concentrations. In addition, its phase diagram in water and in saline solutions has been studied by means X-ray and SANS experiments [16–20]. In the dilute part of the diagram the micellar phase predominates at AOT mass fractions below 1.4%, while between 1.4 and 10% micelles are in equilibrium with vesicles; finally up to 10% of AOT mass fractions the existence of a single lamellar domain is not clear [16]. From these results one can conclude that even though the phase diagram of aqueous AOT has been presented, the surfactant dilute region need to be clarify by obtaining the size or the critical concentration by means of techniques more sensitive to concentration that SANS. Therefore, in previous works we have characterized the dilute region determining the critical concentration of vesicles for pure AOT and for binary mixtures of AOT with poly(ethylene glycol), PEG 17 kDa, NaCl and poly(sodium 4-styrene sulfonate), PSS [21,22]. Results showed that the addition of PSS, PEG and NaCl decreases the aggregation critical concentrations [21]. However, the effect induced by additives is different; in the case of PSS and NaCl, there is a screening of the surface charge while the adsorption of PEG molecules at the interface seems to be responsible for the decrease of the aggregation concentration [22]. In these works, the polymer concentration was always in the dilute regime. However, we are interested to investigate systematically the effects of both, polymer concentration and mass on the stability of vesicles. Therefore, we have expanded the PEG concentration at the semidilute regime and the polymer mass from 6 kDa (PEG 6k) to 35 kDa, PEG 35k. Taking into account that the structure of the interface plays an important role on vesicle stability [23,24], we have obtained the properties of the vesicle interfaces by means of fluorescence probing and electrokinetic's measurements [22]. Finally, using dynamic light scattering measurements and cryogenic transmission electron microscopy, Cryo-TEM we determine the size and the morphology of surfactant aggregates without and with polymers.

2. Materials and methods

2.1. Reagents and vesicle preparation

The surfactant sodium bis(2-ethyl-hexyl) sulfosuccinate was purchased from Fluka and was purified according to the published method [24]. The purity was evaluated by using gas chromatography [25]. The results indicate that the samples contain <0.5% (w/w) of 2-ethyl hexanol. This alcohol is formed by hydrolysis of either one or both of the two hydrocarbon tails.

Poly(ethylene glycol) fractions PEG 6k, PEG 17k, and PEG 35k were used as received and the molecular weight provided by the manufactured (Fluka) were 6, 17 and, 35 kDa, respectively. Nabumetone, 4-[6-methoxy-2-naphthyl]- 2-butanone was from Sigma Chemical Co. and was used as received without further purification.

The pure vesicles were prepared by adding the calculated amount of surfactant to the solvent, water. In polymer–surfactant mixtures, the surfactant was dissolved in the aqueous polymer solution with a given concentration. The most dilute solutions were prepared by dilution from the stock concentrated solution. In all cases, care is taken not to use external energy input except a gentle stirring.

The solutions were prepared with water purified with a combination of RiOs and Milli-Q systems from Millipore. All solutions were prepared the day before to obtain experimental measurements and were maintained at 30 °C. At this temperature, all solutions are clear.

2.2. Steady-state fluorescence measurements

The emission spectra of nabumetone incorporated to AOT vesicles were recorded with the LS-50B spectrofluorometer from Perkin–Elmer. The concentration of nabumetone was kept constant at a value of 4×10^{-5} M. The excitation wavelength was 317 nm and the excitation and emission slits were 2.5/2.5 or 3/3 nm depending of the fluorescence intensity. The instrumental response at each wavelength was corrected by means of the curve provided with the spectrofluorometer. The fluorescence quantum yield, Φ, was calculated using quinine sulfate in 0.1 N sulphuric acid as reference [26] ($\Phi_{\text{ref}} = 0.543$). The spectra were recorded at 30.0 °C.

2.3. Zeta potential measurements

The Zetasizer 3000 device (Malvern, UK) was used to carry out the electrophoretic mobility of vesicles. This apparatus uses laser-Doppler velocimetry to measure the electrophoretic mobility, μ_e. All experiments were made in a 5 mm × 2 mm rectangular quartz capillary. Each experimental value is the average of ten measurements and the standard deviation of these measurements was considered the experimental error. The electrophoretic mobility values were also obtained at 30.0 °C.

2.4. Light scattering measurements

Dynamic light scattering were performed with an CGS-8 from ALV GmbH working in pseudocross-correlation mode, using the green line ($\lambda = 514.5$ nm) of an argon ion laser (Coherent I300). The intensity correlation functions were obtained at a fixed temperature of 30.0 °C and as a function of the scattering angle, θ, between 30 and 140 °C, corresponding to wavevectors, q, from 8.42×10^4 to 3.14×10^5 cm^{-1} defined as

$$q = \frac{4\pi n}{\lambda} \sin\left(\frac{\theta}{2}\right),$$

where n is the solution refractive index.

The normalized second order correlation functions ($g^{(2)}(t)$) were analyzed using both GENDIST [27] and CONTIN [28] inverse Laplace algorithms, giving both similar relaxation time distributions. From the average relaxation times, τ, the apparent diffusion coefficients, D^{app}, were obtained and using the Stokes–Einstein relation, the apparent hydrodynamic radii were calculated [29]:

$$1/\tau = D^{\text{app}} q^2 = \frac{k_B T}{6\pi\eta R_H^{\text{app}}} q^2.$$

2.5. Cryogenic transmission electron microscopy, Cryo-TEM

Cryo-transmission electron microscopy is a particular technique for the direct visualization that has been used to obtain direct high resolution images of surfactant aggregates such as micelles, vesicles and different structures formed in polymer–surfactant systems [30,31]. The sample (0.1 μl) was deposited on a carbon-coated holey polymer film in a controlled environment vitrification system, (CEVS) Gatan cryoplunge, where temperature and relative humidity are controlled. The excess liquid is blotted away with filter paper and quickly vitrified in liquid ethane. The sample is then transferred to a JEOL JEM 2010 FEG electron microscope by means of a Gatan CT 3500 Cryo-transfer system. The observations were made to an acceleration voltage of 200 kV. The working temperature was −170 °C and the images were recorded on a digital camera Gatan MSC794. The pictures were taken at a certain defocus to obtain high-quality images.

3. Results and discussion

3.1. Steady-state fluorescence measurements

The emission spectra of nabumetone dissolved in Aerosol OT vesicles and in AOT–polyethylene glycol vesicles were obtained. Some of these spectra are represented in Fig. 1. As can be seen in the figure the nabumetone emission spectrum consists in a broad band centered at 350 nm and the emission intensity increases as the surfactant concentration also increases. To quantify differences between emission intensity, the fluorescence quantum yields, Φ_f, is preferred to fluorescence intensity; then the variation of Φ_f with surfactant concentration is represented in Fig. 2. Results represented in the figure correspond to mixed vesicles of AOT and PEG 6k, similar behavior is observed in all mixtures studied. For the sake of clarity, the fluorescence quantum yield of nabumetone dissolved in mixed polymer–surfactant aggregates was normalized respect to the quantum yield of nabumetone dissolved in aqueous polymer solution (Φ_0) with polymer concentration match those in the AOT solutions.

Results presented in Fig. 2 show that the quantum yield of nabumetone increases with AOT concentration until it reaches a plateau at a particular surfactant concentration, cvc, corresponding to the vesicle formation. The cvc is obtained from the interception of quantum yield values above and below the

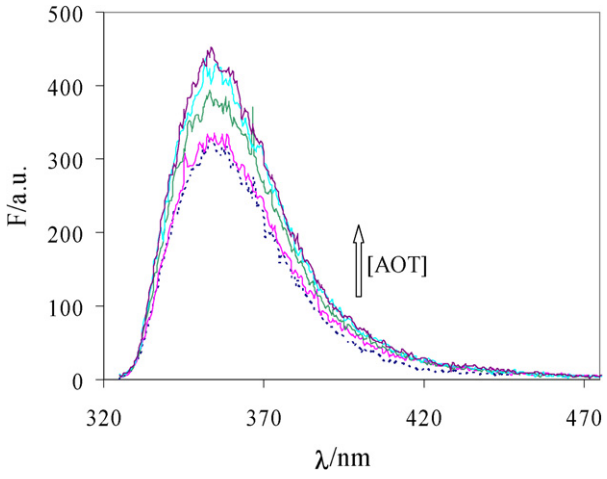

Fig. 1. Fluorescence spectra of nabumetone solubilized in vesicles of AOT with 0.6% PEG 17k containing different surfactant concentration. Dotted line is the fluorescence spectrum of nabumetone dissolved in aqueous polymer solution.

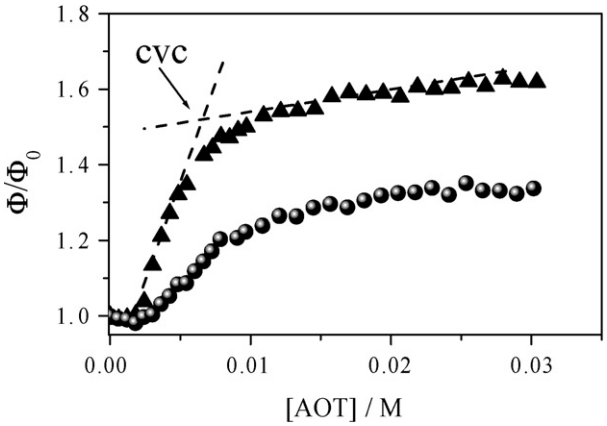

Fig. 2. Effect of the AOT concentration on the fluorescence quantum yield of nabumetone solubilized on AOT/PEG 6k aggregates: triangles [PEG 6k] = 1% and circles [PEG 6k] = 10%. The quantum yield is normalized respect to that of nabumetone dissolved in polymer solutions, see text.

cvc, see Fig. 2. The cvc values found using this method acceptably agree with those obtained from conductivity or surface tension measurements [21]. Differences between the cvc values obtained with distinct techniques were analyzed elsewhere [22] and shown that the quantum yield of nabumetone can be used to estimate the cvc of vesicles [22]. As can be seen in the figure, the nabumetone quantum yield increases more sharply in aggregates dissolved in dilute polymer solutions.

The photochemical behavior of this probe has been studied [32] and the results indicated that nabumetone exists in two conformations, the folded conformation, low Φ_f, responsible for the fluorescence quenching of the naphthalene ring by the butanone side chain, and the extended conformation with high Φ_f. The folded conformation predominates in aqueous solutions [32] (≈91%). According to values found, in the most dilute surfactant solutions the folded conformation predominates, while at high surfactant concentrations, the probe is transferred to a more hydrophobic microenvironment, and the quantum yield increases. Finally, when the AOT concentration reaches the cvc the probe nabumetone is incorporated

Table 1
Critical vesicle concentration values found for Aerosol OT vesicles

Additive	1% PEG 6k	10% PEG 6k	0.6% PEG 17k	10% PEG 17k	1% PEG 35k	5% PEG 35k
cvc (mM)	6.5	9.9	6.8	10.4	6.4	8.5

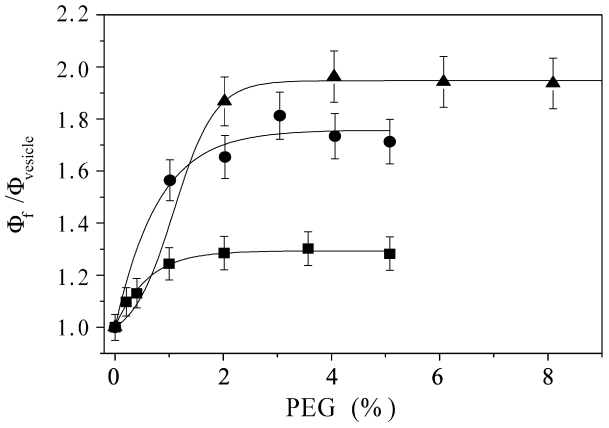

Fig. 3. Effect of polymer concentration on the fluorescence quantum yield of nabumetone solubilized in AOT/PEG aggregates: (triangles) PEG 6k, (squares) PEG 17k and (circles) PEG 35k. The AOT concentration is 0.03 M. The lines are guide to the eyes.

to the aggregates and the quantum yield remains constant. In a previous work, nabumetone was successfully used [22] to determine the critical concentration of pure vesicles of AOT and mixed vesicles formed by AOT and a water-soluble polymer, PSS or PEG 17k. In the work, the polymer solutions are always in dilute regime. The cvc is evaluated from the nabumetone quantum yield vs surfactant concentration curves and the values are collected in Table 1. Taking into account that the cvc of pure AOT vesicles is 7.3 mM [21,22], the cvc values show two different trends, for dilute polymer solutions the cvc decreases as compared with pure AOT vesicles. This classical behavior in polymer–surfactant mixtures indicates the existence of polymer–surfactant interactions responsible of the stabilization of the aggregates [33]. This fact is consistent with results obtained elsewhere for AOT/PEG 17k in dilute polymer solutions [22]. Conversely, when polymer concentration increases up to a certain value the cvc is higher than that for pure AOT vesicles. In addition, the nabumetone quantum yield increases more sharply in aggregates dissolved in dilute polymer solutions. These facts seem to indicate the existence of two different aggregation processes.

Fig. 3 presents the variation of nabumetone quantum yield with polymer concentration. The AOT concentration is kept constant at 0.03 M. In the figure, we represent the ratio between the fluorescence quantum yield of nabumetone dissolved in AOT/PEG mixtures and dissolved in pure vesicles of AOT, referred as Φ_{vesicle}. The quantum yield of nabumetone increases as the polymer concentration increases and it reaches a constant value at a certain polymer concentration: 2.7% for PEG 6k, 1.5% for PEG 17k and 2.5% for PEG 35k. All these facts seem to indicate the existence of different aggregation processes depending on polymer concentration. In particular, one could hope that the anchored polymer molecules destabilize the vesicle and lead to the formation of different kind of aggregates.

From fluorescence results, the polymer concentrations corresponding to vesicle–micelle transition do not present a monotonic behavior with the polymer molecular weight. Thus, the vesicle–micelle transition seems to be favored by the addition of PEG molecules of intermediate weight, PEG 17k. This fact can be due to the preferential adsorption of this polymer at the vesicle surface. The polymer coverage of the vesicle surface may be controlled by varying polymer concentration or varying polymer size. The anchoring free energy of a polymer molecule consists in two main components [34] the energy gained by inserting the polymer into the surfactant monolayer and the entropy lost by constraining the chain by the surface. These components have an opposite dependence on the polymer mass; consequently, the polymer adsorption goes through a maximum at a certain polymer size [34].

We also analyze the effect of the polymer molecular weight on the quantum yield of nabumetone. As can be seen in Fig. 3, the lowest quantum yield values correspond to mixtures with PEG 17k, while no very significant differences are observed on the quantum yield values of aggregates with PEG 6k and PEG 35k. This fact can be explained if one takes into account that nabumetone is strongly quenched by water [32] and that nabumetone is located at the vesicle interface [22]. Thus, the low the quantum yield values in systems with PEG 17k can be due to an increase of the hydration of the surfactant head group at the interface. Baran et al. [35] showed that different hydration levels can be induced by the adsorption of PEG and correspond with two PEG structural configurations: the PEG molecules adsorbed in form of random coil, low hydration level, and the strongly adsorbed polymer molecules giving a brush structure, highly hydrated surface. Thus in our systems, the fluorescence results seem to indicate that PEG 17k induces higher hydration on the vesicle surface than PEG 6k or PEG 35k. This fact is probably due to the stronger adsorption of this polymer at the interface.

All these results clearly show that the properties of vesicle interface plays and important role on the stability of aggregates. This is consistent with theoretical predictions [12] and experimental observations [36]. To obtain more information about the interface of the different aggregates the electrophoretic mobility was obtained.

3.2. Electrophoretic mobility results

The effect of the addition of PEG polymers on the electrophoretic mobility of AOT vesicles was investigated and the results are presented in Fig. 4. The electrophoretic mobility curves decreases as the polymer concentration increases and the effect is more pronounced in PEG 17k. The diminution of the electrophoretic mobility by the addition of polymers was

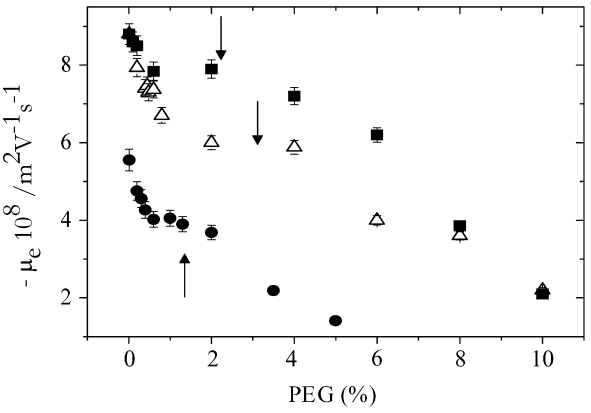

Fig. 4. Effect of the mixture composition on the electrophoretic mobility of vesicles composed of 0.03 M of AOT and variable polymer concentrations: PEG 6k (triangles), PEG 17k (circles) and PEG 35k (squares). The arrows point the polymer concentration at which the fluorescence quantum yield reaches a constant value.

previously observed for AOT/PEG 17k in dilute polymer concentrations, and was interpreted using the diffuse double layer theory [22]. According to it, the PEG adsorption on the interface gives a relatively thick layer on the surface, which shifts the slip boundary toward the bulk solution decreasing the electrophoretic mobility [22,35].

In all these systems, when the polymer concentration increases, the electrophoretic mobility decreases in absolute value and reaches a plateau. The end of the plateau corresponds to the polymer concentration at which the fluorescence quantum yield reaches a constant value, arrows in Fig. 4. A further polymer addition gives smaller absolute values of μ_e that may be an indication of the transition from vesicles to micelles.

The electrophoretic mobility measurements are consistent with fluorescence results. Thus, the aggregates with PEG 17k present the smallest electrophoretic mobility in absolute value. This fact indicates that PEG 17k forms the densest polymer layer responsible of both the lowest quantum yield values of nabumetone and the lowest electrophoretic mobility in absolute value.

3.3. Light-scattering measurements

In order to obtain information on the effect of polymer addition on aggregates size, dynamic light-scattering experiments have been performed at 30.0 °C with different polymer concentrations, and keeping constant the AOT (0.03 M). For comparative purposes, the size of pure components, AOT aggregates and aqueous polymers were determined. In the former the AOT concentration is also 0.03 M and in the latter, the polymer concentrations were the highest used in mixed systems, which in all cases is well above the overlapping concentration [37], ($c*$(PEG 35k) = 0.9% w/w, $c*$(PEG 17k) = 1.4% w/w, $c*$(PEG 6k) = 3% w/w).

Both pure AOT and PEG solutions give single exponential correlation functions (Fig. 5A) that, when analyzed using regularized inverse Laplace transforms (ILT) (GENDIST, CONTIN), lead to single peak decay time distributions (Fig. 5A). The inverse decay time (Fig. 5B) shows the expected q^2 dependence in the case of the polymer, while for AOT shows a non q^2 only above a scattering angle of 100 °C.

In the case of vesicles the non q^2 behavior has been predicted when Helfrich interfacial elasticity is properly considered in the calculation of the scattering function [38], a more detailed study on this matter will be presented in a future paper.

All the experiments corresponding to mixtures present multiexponential correlation functions and the ILT treatment gives complex distribution functions. Fig. 6 presents the distribution function, on the apparent hydrodynamic radius scale (R_H^{app}), for two different concentrations of PEG 6k and illustrates the behavior found for the rest of polymer molecular weights.

At low polymer concentrations the distribution functions show two components, the one corresponding to the highest radius, shows similar q^2 inverse decay time dependence to the pure AOT vesicles, with a apparent hydrodynamic radius of (57.7 ± 0.6 nm). The second component corresponds to the lowest radius and has the expected q^2 dependence for all the scattering angles. The average radius (6.6 ± 0.4 nm) found for this component is compatible with an elongated micellar aggregate. Table 2 collects the rest of the R_H^{app} values along with the amplitudes of the different modes at the scattering angle of 90 °C.

At high polymer concentrations, the distribution functions also show two components, both have linear inverse decay time q^2 dependences. The average R_H^{app} values found for 10% PEG 6k ([AOT] = 0.03 M) were 1.5 ± 0.1 nm and 299 ± 4 nm, and in Table 2 are collected the rest of the values. The size of the lowest component is compatible with spherical micelles while the highest size component may correspond to very large rod like micelles or to superstructures of elongated micelles embedded in a polymer network.

3.4. Cryo-transmission electron microscopy, Cryo-TEM

To reveal the structures formed at different AOT–polymer compositions and to help elucidate the light scattering results, the systems were analyzed by means of Cryo-TEM. This technique allows direct examination of microstructures after rapid freezing of the hydrated specimens. Cryo-TEM pictures obtained from an aqueous solution of Aerosol OT 0.01 M are in Fig. 7. We have obtained a large number of pictures from aqueous solutions of 0.01 and 0.03 M of AOT; pictures showed in Fig. 7 were chose for the high quality of images and because are the most representative of the size distribution of AOT vesicles. The figure shows that monodisperse small unilamellar vesicles, SUV, with a radius of about 20 nm predominate in this system. Fig. 7b also shows the existence of multilamellar vesicles, MLV, in a small proportion as compared with AOT vesicles. The biggest aggregates were observed by optical microscopy [21]. Fig. 7c shows the distribution of the outer vesicle diameter for 200 vesicles taken for Cryo-TEM. Results show an almost monomodal distribution of vesicles. Qualitatively, the light scattering results agree with Cryo-TEM ones showing that Aerosol OT solutions consists in rich monodisperse vesicles system. However, the radius measured by light scat-

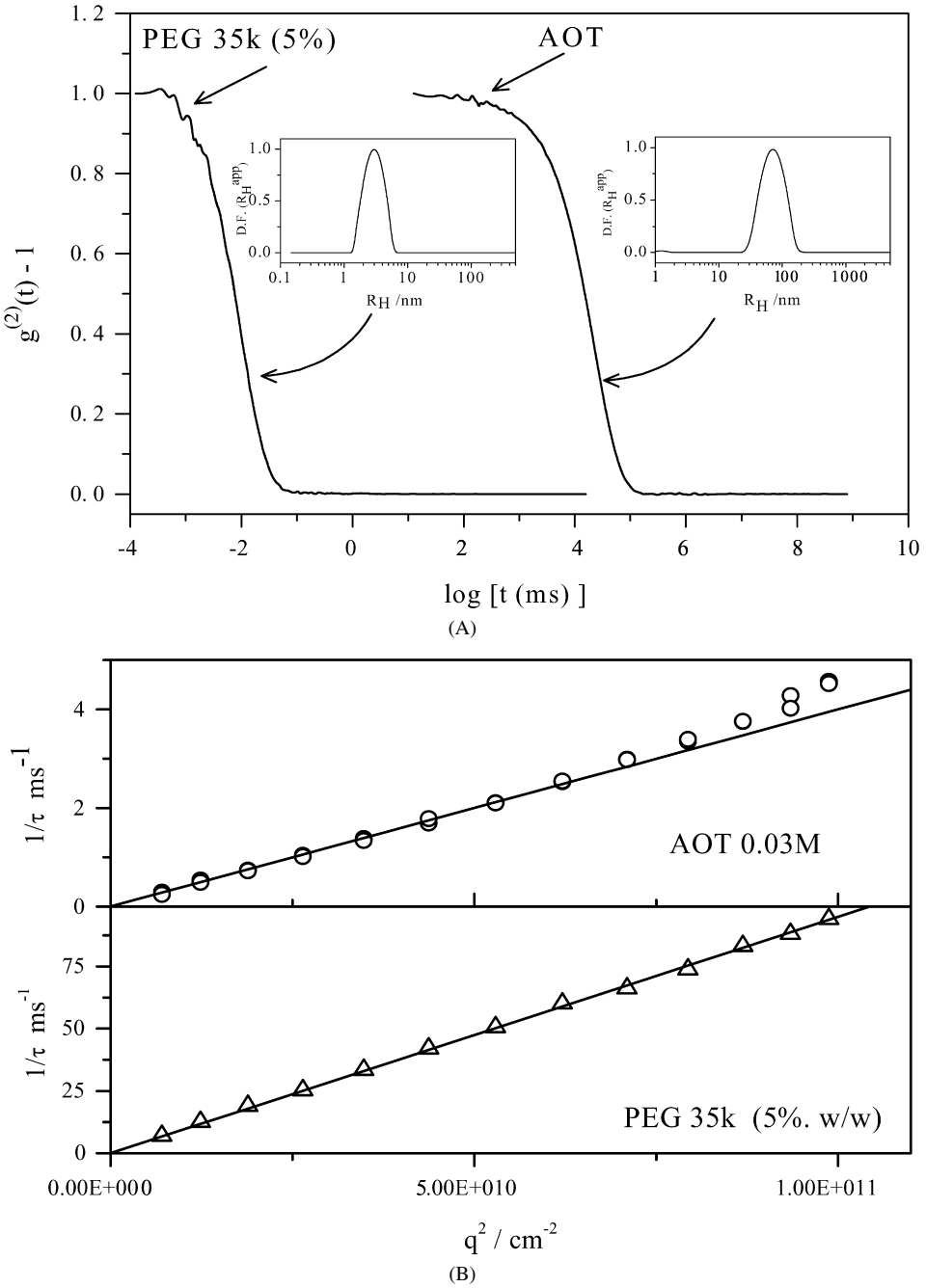

Fig. 5. (A) Normalized second order correlation functions, $g^{(2)}(t)$, and (B) the inverse decay time values vs the square wavevectors for pure AOT 0.03 M and for pure PEG 35k (5% w/w).

tering ($R_H = 68.5$ nm, for AOT 0.01 M), is significantly larger than the radius measured by Cryo-TEM (diameter = 40 nm). This can be partly because scattering yields an intensity average while Cryo-TEM gives a number average and so the former weights larger aggregates that scatter more light and shifts the hydrodynamic radius toward larger values [39,40].

Cryo-TEM images for AOT solutions with polymer concentrations above the overlapping one show that the system is formed by spherical micelles with a micelle radius between 2.5 and 3 nm in agreement with light scattering results. In addition, some large aggregates of different size were observed.

In dilute polymer solutions, below the overlapping one, Cryo-TEM shows no clear images, probably due to vesicle association in the freezing process and the formation of too big assemblies [41]. Thus, we use Cryo-etch SEM to confirm this fact. The procedure of preparation of samples and some of these images are in Supplementary material section. The pictures show big colloidal assemblies probably due to vesicle association in the freezing process. The formation of aggregates of similar structure was observed in saline surfactant solutions [42] or in binary colloidal systems [41]. The structure of these assemblies is independent of the freezing procedure and preserves some vesicles inside the colloidal aggregates.

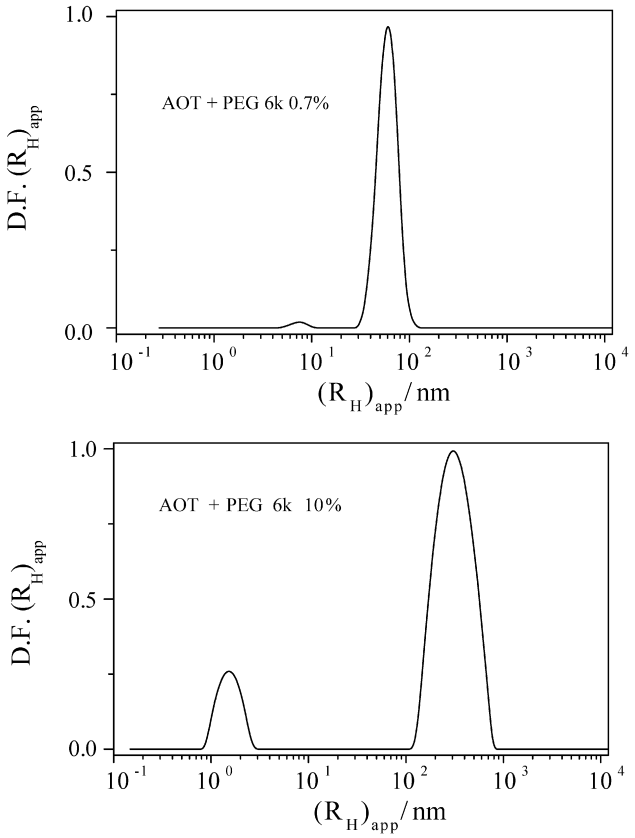

Fig. 6. Distribution functions on an apparent hydrodynamic radius scale for AOT 0.03 M and two different concentrations of PEG 6k.

Table 2
Apparent hydrodynamic radius and amplitude values found using dynamic light scattering for aggregates formed in Aerosol OT and PEG polymers in aqueous solutions

Additive	R_H (nm)	A_1 (%)	R_H (nm)	A_2 (%)	R_H (nm)	A_3 (%)
0	67.3 ± 0.4	100				
0.07% PEG 6k	57.7 ± 0.06	99	6.6 ± 0.4	1	–	–
10% PEG 6k	–	–	1.5 ± 0.1	18.8	299 ± 4	81.2
0.2% PEG 17k	71 ± 0.9	72	3 ± 0.5	28	–	–
0.4% PEG 17k	60.5 ± 0.06	48	2.4 ± 0.05	52	–	–
10% PEG 17k	–	–	1.7 ± 0.02	11	882 ± 12	89
0.4% PEG 35k	74 ± 2	95.3	3.4 ± 0.1	4.7	–	–
5% PEG 35k	–	–	2.4 ± 0.2	16	398 ± 10	84

Note. Amplitudes of the different modes, A_i, correspond to 90° while the R_H values are obtained from the inverse decay rate vs square wave vector plots.

Cryo-TEM and light scattering results indicate that monodisperse small unilamellar vesicles (SUV) form pure AOT solutions. The addition of small concentrations of PEG 6k, PEG 17k and PEG 35k leads to the appearance of elongated micelles coexisting with SUV's. With a further increase in PEG content, SUV disappears and the size of the elongated micelles decreases to a radius compatible with spherical micelles. For the highest PEG concentrations all the polymers are well above the overlapping concentration, in these cases coexisting with spherical micelles, very large aggregates have been detected. These aggregates may correspond to very large rod like micelles

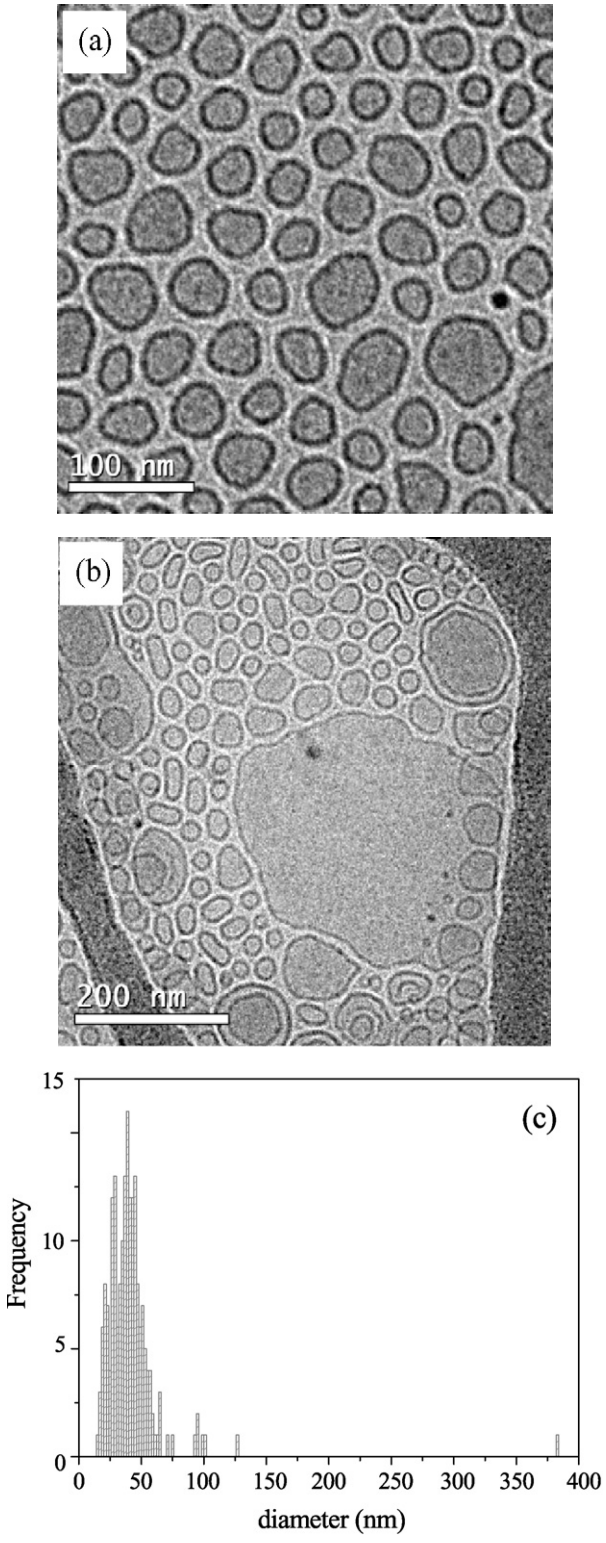

Fig. 7. Cryo-TEM micrographs from an aqueous solution of Aerosol OT 0.01 M sample; (a) monodisperse small vesicles area; (b) multilamellar and small vesicles area; (c) histogram of vesicle sizes from Cryo-TEM images.

or to superstructures of elongated micelles embedded in a polymer network. According to the results found in this work, the addition of PEG on AOT water solutions induces the following transitions:

$$\text{SUV} \xrightarrow{+\text{PEG}} \text{SUV} + \text{elongated micelles}$$
[dilute polymer regime]

$$\xrightarrow{+\text{PEG}} \text{Spherical micelles} + \text{large aggregates}$$
[semidilute polymer regime].

Fluorescence and electrophoretic measurements seem to indicate that these transitions are due to the polymer adsorption at the vesicle interfaces. The polymer adsorption increases the area of the surfactant at the interface, consequently, the vesicles → micelles transition can be interpreted in terms of the packing parameter, $P = v_c/al_c$. In this equation, v_c and l_c represent the volume and the length of the surfactant hydrocarbon chain, respectively and a is the area of the surfactant at the interface. When both mass and polymer concentration increase, P decreases because the area of surfactant increases with polymer adsorption and going from AOT vesicles, $P = 0.63$ ($1 > P > 1/2$), rod-like micelles ($P > 1/3$) and finally spherical micelles for ($P < 1/3$).

4. Conclusions

We were interested to analyze the effect of the polymer size and concentration on the vesicle stability and size in order to clarify the mechanism of formation of stable vesicles of a well-defined size with possible applications in formulations. In previous works, the authors studied the effect of polymer addition on the vesicles produced using an input of energy; however, we think that the input of energy could affect the vesicle stability and therefore we chose the surfactant AOT because it forms spontaneous vesicles. We have demonstrated that the addition of PEG polymers induces vesicles → micelles transition and that this transition takes place via intermediate structures such as elongated micelles of different sizes. The results also indicate that the driving force for the vesicle–micelle transformation seems to be the formation of a PEG layer adsorbed at the interface; consequently, PEG molecules with the highest adsorption ability favor the vesicle transformation. We also demonstrate that the polymer molecular weight and the polymer concentration modify the size and distribution of the AOT aggregates.

Acknowledgments

The work was financially supported by Ministerio de Ciencia y Tecnología (BQU 2001-1507) and Ministerio de Educación y Ciencia (MAT 2004-04180). The authors acknowledge the C.A.I. of Spectroscopy of the Universidad Complutense de Madrid for making available the light scattering facility and the Microscopía Electrónica de Alta Resolución y Caracterización de Materiales, C.A.C.T.I., of the Universidade de Vigo for the Cryo-TEM and Cryo-SEM facilities. M.M. Velázquez is grateful to Universidad de Salamanca for the partial support of her stay in Madrid.

Supplementary material

The online version of this article contains additional supplementary material: Cryo-etch SEM images of big colloidal assemblies formed in the freezing process in solutions with Aerosol OT and PEG 6k. The surfactant concentration remains constant at 0.03 M AOT while that PEG 6k concentrations were 0.03 and 1%, respectively.

Please visit DOI: 10.1016/j.jcis.2007.09.008.

References

[1] A. Ben-Shaul, in: R. Lipowsky, E. Sackmann (Eds.), Structure and Dynamics of Membranes: From Cells to Vesicles, Elsevier, Amsterdam, 1995, p. 359.
[2] B. Ceh, M. Winterhalter, P.M. Frederick, J.J. Vallner, D.D. Lasic, Adv. Drug Delivery 24 (1997) 165.
[3] D.F. Evans, H. Wennerström, The Colloidal Domain, second ed., Wiley–VCH, New York, 1999, p. 308.
[4] C. Tondre, C. Caillet, Adv. Colloid Interface Sci. 93 (2001) 115.
[5] (a) E. Marques, A. Khan, M.G. Miguel, B. Lindman, J. Phys. Chem. B 102 (1998) 6746;
(b) E. Marques, A. Khan, M.G. Miguel, B. Lindman, J. Phys. Chem. B 103 (1999) 8353.
[6] M. Villeneuve, S. Kaneshina, M. Aratono, J. Colloid Interface Sci. 262 (2003) 227.
[7] M.I. Viseu, M.M. Velázquez, C.S. Campos, I. García-Mateos, S.M.B. Costa, Langmuir 16 (2000) 4882.
[8] P. De Moor, T. Beclen, B. Komancheck, O. Díaz, R. van Santen, J. Phys. Chem. B 101 (1997) 11077.
[9] S.A. Safran, P. Pincus, D. Andelman, Science 248 (1990) 354.
[10] G. Porte, C. Ligoure, J. Chem. Phys. 102 (1995) 4290.
[11] I. Szleifer, M. Carignano, Adv. Chem. Phys. 94 (1996) 165.
[12] M. Rovira-Bru, D.H. Thompson, I. Szleifer, Biophys. J. 83 (2002) 2419.
[13] G. Blume, G. Cevc, Biochim. Biophys. Acta 1029 (1990) 91.
[14] V.P. Torchilin, V.G. Omelyanenko, M.I. Papisov, A.A. Bogdanov Jr., V.S. Trubetskoy, J.N. Herron, C.A. Gentry, Biochim. Biophys. Acta 1195 (1994) 1.
[15] G. Montesano, R. Bartucci, S. Belsito, D. Marsh, L. Sportelli, Biophys. J. 80 (2001) 1372.
[16] K. Fontell, J. Colloid Interface Sci. 44 (1973) 156.
[17] F.M. Ficheux, A.M. Bellocq, F. Nallet, Colloids Surf. A 123–124 (1997) 253.
[18] M. Skouri, J. Marignan, R. May, Colloid Polym. Sci. 269 (1991) 929.
[19] B. Balinov, U. Olsson, O. Sodermann, J. Phys. Chem. 95 (1991) 5931.
[20] I. Grillo, E.I. Katts, A.R. Muratov, Langmuir 19 (2003) 4573.
[21] J.I. Briz, M.M. Velázquez, J. Colloid Interface Sci. 247 (2002) 437.
[22] M. Valero, M.M. Velázquez, J. Colloid Interface Sci. 278 (2004) 465.
[23] S.A. Walker, J.A. Zasadzinski, Langmuir 13 (1997) 5076.
[24] F.M. Menger, K. Yamada, J. Am. Chem. Soc. 101 (1979) 6731.
[25] S.S. Datwani, K.J. Stebe, Langmuir 17 (2001) 4287.
[26] M.M. Velázquez, M. Valero, L.J. Rodríguez, S.M.B. Costa, M.A. Santos, J. Photochem. Photobiol. B Biol. 29 (1995) 23.
[27] (GENDIST) J. Jakes, Collect. Czech. Chem. Commun. 60 (1995) 1781.
[28] (a) (CONTIN) S.W. Provencher, Comput. Phys. Commun. 27 (1982) 213;
(b) (CONTIN) S.W. Provencher, Comput. Phys. Commun. 27 (1982) 229.
[29] Handbook of Chemistry and Physics, 60th ed., CRC Press, Boca Raton, FL, 1980.
[30] P.K. Vinson, J.R. Bellare, H.T. Davis, W.G. Miller, L.E. Scriven, J. Colloid Interface Sci. 141 (1991) 74.
[31] M. Almgren, K. Edwards, J. Gustafsson, Curr. Opin. Colloid Interface Sci. 1 (1996) 270.
[32] M. Valero, S.M.B. Costa, M.A. Santos, J. Photochem. Photobiol. A Chem. 132 (2000) 67.
[33] E.D. Goddard, Colloids Surf. 19 (1986) 255.
[34] Y. Barenholz, Curr. Opin. Colloid Interface Sci. 6 (2001) 66.
[35] A.A. Baran, N.M. Soboleva, L.M. Dukina, Kolloid Z. 46 (1983) 840.

[36] K. Hristova, A. Kenworthy, T.J. McIntosh, Macromolecules 28 (1995) 7693.
[37] S.U. Egelhaaf, M. Müller, P. Schurtenberger, Langmuir 14 (1998) 4345.
[38] M. Hosek, J.X. Tang, Phys. Rev. E 69 (2004) 1.
[39] C. Ladaviere, M. Touston, Y. Gulik-Krzywicki, C. Tribet, J. Colloid Interface Sci. 241 (2001) 178.
[40] M.L. Ferrer, R. Esquembre, I. Ortega, C.R. Mateos, F. del Monte, Chem. Mater. 18 (2006) 554.
[41] I. Szleifer, O.V. Gerasimov, D.H. Thompson, Proc. Natl. Acad. Sci. 95 (1998) 1032.
[42] F.M. Menger, H. Zhang, K.L. Caran, V.A. Seredyuk, R.P. Apkarian, J. Am. Chem. Soc. 124 (2002) 1140.